Adsorption (2019) 25:201–216
https://doi.org/10.1007/s10450-019-00028-2

Analytical model and experimental investigation of the adsorption thermodynamics of coalbed methane

Haijian Li[2] · Guanghua Li[2] · Jianhong Kang[1,2] · Fubao Zhou[1,2,3] · Jinchang Deng[2]

Received: 15 May 2018 / Revised: 24 January 2019 / Accepted: 30 January 2019 / Published online: 20 February 2019

Abstract

The study on adsorption thermodynamics is conducive to a deep understanding of the heat and mass transfer mechanism of coalbed methane in a coal seam. In this work, the analytical expressions of the isosteric heat for six adsorption models taking into account the temperature variations are directly derived according to Clausius–Clapeyron equation. Meanwhile, the adsorption content and adsorption heat at different pressures and temperatures are measured by the volumetric method of adsorption with a microcalorimetry system. It is found that the the adsorption heats obtained by different adsorption models exhibit different trends. The fitting quality of the experimental isotherms for different adsorption models affects the adsorption heat result. However, even if the models well fit the experimental isotherms, the theoretical adsorption heat values may be inconsistent. Furthermore, the calorimetric heats for all coal samples decreases with the increase in adsorption content in relation to the micropore distribution of coal. For all coal samples, the modified Dubinin–Astakhov (D–A) model can well fit the experimental isotherms and agree well with the results of calorimetric heats. By comparing the theoretical heat for different k values and the measured heat, the pseudo-saturation vapor pressure of the modified D–A model can be determined. Finally, by virtue of the isosteric heat of adsorption in a small temperature range, the adsorption isotherms at other adjacent temperatures are predicted successfully.

Keywords Adsorption · Isosteric heat · Coalbed methane · Coal

1 Introduction

Coalbed methane (CBM), which mainly consists of methane, has been increasingly recognized as a clean unconventional natural gas resource, most of which is stored in an absorbed state in coal seams. In recent years, the adsorption mechanism of CBM has been an important research field for the engineering application of CBM (Tang et al. 2015). The adsorption capacity of coal can be simply reflected by the adsorption content of methane. There are several theoretical and experimental studies on the adsorption content of methane in coal and its relationship with the characteristics of the coal (e.g., coal rank, maceral and mineral composition, pore structure, proximate analysis indices and functional group content) (Moore 2012; Busch and Gensterblum 2011; Bustin and Clarkson 1998; Dutka et al. 2013). However, simple research on the adsorption content is insufficient to understand the adsorption mechanism of CBM. The adsorption content cannot directly reflect the thermodynamic properties of adsorption, such as the adsorption heat (Chattaraj et al. 2016). One of the most important types of adsorption heat is isosteric heat, which can provide unique information on the adsorption intensity, adsorption type and adsorption process (Horikawa et al. 2015; Do et al. 2008; Madani et al. 2015). In general, the isosteric heat of physical adsorption is < 40 kJ/mol, whereas the chemical adsorption is > 40 kJ/

Electronic supplementary material The online version of this article (https://doi.org/10.1007/s10450-019-00028-2) contains supplementary material, which is available to authorized users.

✉ Jianhong Kang
jhkang@cumt.edu.cn

✉ Fubao Zhou
f.zhou@cumt.edu.cn

[1] Jiangsu Key Laboratory of Fire Safety in Urban Underground Space, China University of Mining and Technology, Xuzhou 221116, China

[2] School of Safety Engineering, China University of Mining and Technology, Xuzhou 221116, China

[3] State Key Laboratory of Coal Resources and Safe Mining, China University of Mining and Technology, Xuzhou 221116, China

mol. The analysis of adsorption thermodynamics is helpful for understanding the microscopic mechanism and energy transformation process of adsorption of CBM on the coal surface. In addition, the thermal effect caused by the adsorption heat of CBM affects the coal's temperature (Liu et al. 2014; Yue et al. 2015). The thermodynamic characteristics of CBM adsorption are also notably important for understanding the heat and mass transfer mechanism of CBM in coal seams.

Because of the simplicity of its experimental device, the sorption isosteric method is most commonly used to obtain the isosteric heat (Kloutse et al. 2015). This method is based on a certain thermodynamic model such as Clausius–Clapeyron equation, and the isosteric heat is calculated using the adsorption isotherm data at several different temperatures. Some studies focused on the adsorption heat of methane using the sorption isosteric method based on Clausius–Clapeyron equation. Chikatamarla and Crosdale (2001) calculated the isosteric heats of methane in numerous dry Australian coals using the BET model and found isosteric heat values close to 8.8 kJ/mol. Using the results of isothermal tests at 243.15–303.15 K, Tang et al. (2015) obtained the mean isosteric heat of methane in anthracite, lean coal and gas-fat coal, which was 23.31 kJ/mol, 20.47 kJ/mol and 11.14 kJ/mol, respectively. Liang et al. (2016) processed the isothermal adsorption test data at 308 K, 323 K and 338 K conditions using Dubinin–Astakhov (D–A) isotherm model and obtained the initial isosteric heat of methane on montmorillonite, kaolinite, illite and chlorite as 26.088 kJ/mol, 25.543 kJ/mol, 20.503 kJ/mol and 24.229 kJ/mol, respectively. Duan et al. (2016) processed the isothermal adsorption test data at 278–318 K and obtained the initial isosteric heat of methane on shale as 21.58 kJ/mol. Since Clausius–Clapeyron approximation ignores the adsorbed phase effect and uses the ideal gas law, the calculated results may not be reliable, and Clapeyron equation may be more suitable (Pan et al. 1998; Askalany and Saha 2017). According to Clapeyron relationship, Tang et al. (2017) calculated the isosteric heat of methane in Longmaxi shale using the dual-site Langmuir adsorption model.

The calculation of adsorption heat in the literature is chaotic. For example, in some studies, the excess adsorption amounts were directly used (Tang et al. 2015; Duan et al. 2016), whereas others used the absolute adsorption amount (Liang et al. 2016; Tang et al. 2017). Clausius–Clapeyron thermodynamic equation can be found in most studies, but few studies are based on Clapeyron equation. In most studies, only a single adsorption isotherm model was used to calculate the adsorption heat, but using different isotherm models may cause large deviations. Different thermodynamic models, adsorption isotherms and isotherm model may affect the adsorption heat results. At present, there are few studies to compare the results of different thermodynamic and isotherm models, and these results are not verified by other experimental methods. In addition to the sorption isosteric method, the adsorption calorimetry is an effective experimental method to directly obtain the adsorption heat (Siperstein et al. 1999; Zimmermann and Keller 2003). In this method, the integral heat data are collected at different pressures using a calorimeter, and the adsorption content is simultaneously measured using the volumetric method. At present, few studies use the adsorption calorimetry method to study the adsorption heat of CBM. In this paper, the adsorption heat of methane is studied using the sorption isosteric and direct calorimetry method. The adsorption heat results with different thermodynamic and isotherm models and calorimetric heat of methane in coals are compared to provide a reference for the reasonable determination of the adsorption heat of CBM.

2 Thermodynamic models

Because adsorption process is exothermic, the enthalpy change of the adsorption is negative. The adsorption heat is the positive value of the enthalpy change of adsorption (Stadie et al. 2013; Wu et al. 2016). Although ΔH is often used to denote the adsorption heat (Liang et al. 2016; Tang and Ripepi 2017), the enthalpy change of the adsorption may be also expressed by ΔH (White et al. 2005). So q_{st} is used to denote the adsorption heat in this work, and it is always positive in the references (Bhadra et al. 2012; Baran et al. 2014; Pan et al. 1998; Nieszporek 2002). For a certain adsorption amount in the adsorption equilibrium state, Clapeyron equation can be obtained based on thermodynamics as follows (Chakraborty et al. 2006)

$$\frac{dp}{dT} = \frac{q_{st}}{T(v_g - v_a)} \tag{1}$$

where p is the equilibrium pressure (MPa); T is the equilibrium temperature (K); q_{st} is the isosteric heat of adsorption (kJ/mol); v_g and v_a are the molar volumes of the free gas phase and adsorbed phase, respectively (m^3/mol). The isosteric heat of adsorption can be expressed as

$$q_{st} = \frac{dp}{dT} T v_g - \frac{dp}{dT} T v_a \tag{2}$$

If the free gas phase is consistent with the state equation of ideal gas ($pv_g = RT$) and the volume of the adsorption phase is negligible ($v_a \approx 0$), Clausius–Clapeyron equation is obtained (Pan et al. 1998), and the corresponding isosteric heat of adsorption (which is written as q_{st-cc1} in this article) can be expressed as

$$q_{st-cc1} = \frac{dp}{dT} \frac{RT^2}{p} = -R \frac{d \ln p}{d(1/T)} \tag{3}$$

If the free gas phase is consistent with the state equation of real gas ($pv_g = zRT$; z is the gas compressibility factor) and the volume of the adsorption phase is negligible, the corresponding isosteric heat of adsorption (which is written as q_{st-cc2} in this article) can be expressed as

$$q_{st-cc2} = \frac{dp}{dT}\frac{zRT^2}{p} = zq_{st-cc1} \tag{4}$$

Fugacity is usually used to replace pressure for real gas, and the relationship between fugacity and pressure is

$$f = \varphi p \tag{5}$$

where φ is the fugacity cofficient (calcaulated by the Peng–Robinson equation of state in this article).

According to the thermodynamic relationship (the detailed derivation process is shown in the Supporting information), we obtain

$$\frac{dp}{dT} = \frac{1}{\varphi z}\frac{df}{dT} \tag{6}$$

Substituting Eq. (6) into Eq. (4) yields

$$q_{st-cc2} = \frac{dp}{dT}\frac{zRT^2}{p} = \frac{df}{dT}\frac{RT^2}{f} \tag{7}$$

If the free gas phase is consistent with the state equation of ideal gas and the volume of the adsorption phase is not negligible ($v_a \neq 0$), the corresponding isosteric heat of adsorption (which is written as q_{st-c1} in this article) can be expressed as

$$q_{st-c1} = \frac{dp}{dT}\frac{RT^2}{p} - \frac{dp}{dT}Tv_a \tag{8}$$

If the free gas phase is consistent with the state equation of real gas and the volume of adsorption phase is not negligible ($v_a \neq 0$), the corresponding isosteric heat of adsorption (which is written as q_{st-c2} in this article) can be expressed as

$$q_{st-c2} = \frac{dp}{dT}\frac{zRT^2}{p} - \frac{dp}{dT}Tv_a = \frac{df}{dT}\frac{RT^2}{f} - \frac{df}{dT}\frac{Tv_a}{\varphi z} \tag{9}$$

The relationships among the four types of adsorption heat are

$$\frac{q_{st-cc2}}{q_{st-cc1}} = z \tag{10}$$

$$\frac{q_{st-c1}}{q_{st-cc1}} = 1 - \frac{pv_a}{RT} \tag{11}$$

$$\frac{q_{st-c2}}{q_{st-cc2}} = 1 - \frac{pv_a}{zRT} = 1 - \frac{fv_a}{\varphi zRT} \tag{12}$$

$$\frac{q_{st-c2}}{q_{st-cc1}} = z - \frac{pv_a}{RT} = z - \frac{fv_a}{\varphi RT} \tag{13}$$

According to the above thermodynamic relationships, the adsorption heat can be calculated by measuring several isotherms (the relationship between the adsorption content and the pressure at constant temperature). The adsorption content that is directly measured by the volumetric method is called the excess adsorption content (n_{ex}, mmol/g). Since all conventional isotherm equations are based on the absolute adsorption content (n_a, mmol/g), the excess adsorption data cannot be directly fitted (Myers and Monson 2014; Brandani et al. 2017). The absolute adsorption content cannot be directly measured, but it can be calculated from the excess adsorption content (Kim et al. 2011)

$$n_a = n_{ex}/(1 - \frac{\rho_g}{\rho_a}) = n_{ex}/(1 - \frac{v_a}{v_g}) \tag{14}$$

where ρ_g and ρ_a are the densities of the free gas phase and adsorbed phase (kg/m^3); v_g and v_a are the specific volumes of the free gas phase and adsorbed phase (m^3/kg), respectively. It is important to note that v_g and v_a are different from v_a and v_g, although some studies misused Them (Chakraborty et al. 2006; Tang et al. 2017). Their relationship is

$$v_a = \frac{M}{1000}v_a,\ v_g = \frac{M}{1000}v_g \tag{15}$$

where M is the molecular weight for methane (16.0425 g/mol) in this article.

Since the density and volume of the adsorption phase cannot be measured with the current technology, empirical equations for the adsorption phase have been proposed. In this work, we use Dubinin's method and Ozawa's method to calculate the density of the adsorbed phase (Dubinin 1960; Ozawa et al. 1976). The specific volume of the adsorbed phase in Dubinin's method is

$$v_a = \frac{M}{b} \tag{16}$$

where M is the molecular weight for methane (16.0425 g/mol), and b is the constant of van der Waals equation for methane (0.0428 mol). Therefore, the specific volume of the methane adsorption phase is 2.67 cm^3/g.

The specific volume of the adsorbed phase according to Ozawa's method is

$$v_a = v_b \exp\left[\alpha\left(T - T_b\right)\right] \tag{17}$$

where subscripts a and b denote the adsorbed phase and normal boiling point; α is a constant value (0.0025/K); T_b is 111.6 K; ν_b is 2.3585 g/cm^3 for methane. Therefore, the specific volume of the methane adsorption phase is 3.83 cm^3/g, 3.92 cm^3/g and 4.02 cm^3/g at 303.15 K, 313.15 K and 323.15 K, respectively.

The ratio of excess and absolute adsorption contents and the ratio of four types of adsorption heat can be estimated as shown in Fig. 1. The absolute adsorption content is higher

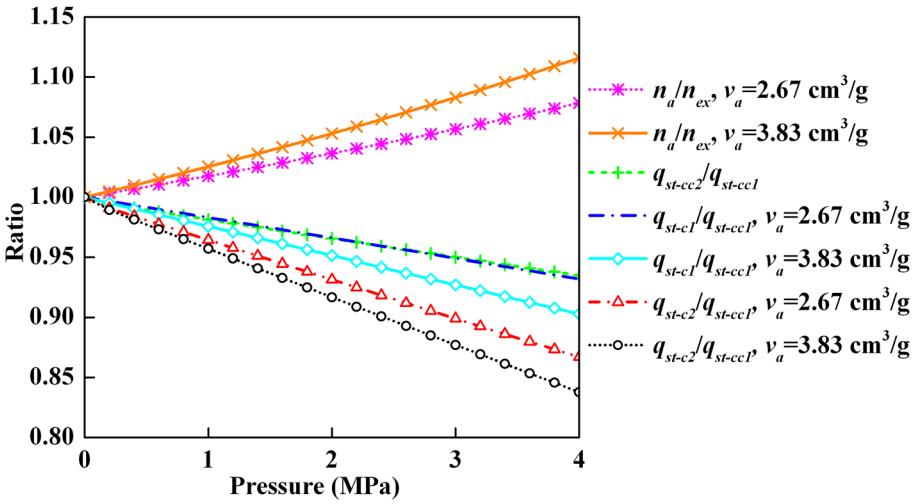

Fig. 1 Effects of the volume of the adsorbed phase on the adsorption uptake and isosteric heat of methane at 303.15 K (data obtained from the NIST REFPROP database)

than the excess adsorption content, and the ratio increases with the increase in pressure. A larger specific volume of the adsorption phase indicates a greater absolute adsorption content. The four types of adsorption heat also have different values. q_{st-cc1} is larger than the other three types of adsorption heat, and the difference increases with the increase in pressure. The specific volume of the adsorption phase also affects the adsorption heat value. A larger specific volume of the adsorption phase correspond to smaller q_{st-c1} and q_{st-c2}. Since the adsorption heat is also affected by the gas compressibility factor, q_{st-c2} is smaller than q_{st-c1}.

The sorption isosteric method must also fit the adsorption isotherm data using isotherm models, and many models have been developed to study the adsorption mechanism of CBM. To fully describe the adsorption, six temperature-dependent adsorption models have been applied to fit the data: Langmuir, Langmuir–Freundlich, Toth, Unilan (Do 1998), Dual-site Langmuir (Bhadra et al. 2012) and Modified Dubinin–Astakhov (D–A) (Richard et al. 2009) equations. In some studies, the isosteric heat was calculated using a graphical method (Ning et al. 2012; Bimbo et al. 2014; Liang et al. 2016). The principle of this method is Clausius–Clapeyron equation. After fitting the isotherms, the pressure points at a given adsorbed amount can be obtained for each T with a simple root finder code using this method. Then, the pressure points can be plotted as ln p versus $1/T$ at the given adsorbed amount, and the isosteric heat can be calculated from the slope of the line. However, this method is effective only when the isosteric heat is independent of the temperature (Bülow et al. 2002). In this paper, the analytical expressions of the isosteric heat of the six different adsorption models are directly derived according to Formula (7) with no assumptions. These analytical expressions are shown in Table 1. By substiting the fitting parameters of the adsorption models into the analytical expressions of the isosteric heat, we can easily obtain the isosteric heat. Due to the same principle, the isosteric heat obtained by the graphical method and analytical method should be identical when the isosteric heat is independent of the temperature or varies little with the temperature. The detailed derivation process is shown in the Supporting information.

3 Experimental methods

3.1 Materials

In this study, three coal samples with different coal ranks were collected from three coal mines in China. According to the mean maximum reflectance of vitrinite, the coal samples are classified from low rank to high rank as: lignite from Donghuai coal mine, gas coal from Beizu coal mine, and anthracite from Chengzhuang coal mine. These coal samples were assigned numbers 1–3 from the highest coal rank to the lowest coal rank. The properties of these coal samples are presented in Table 1. Fresh coals were crushed and sieved, and coal samples of 0.17–0.25 mm were selected for this study. Then, the coal samples were dried at 110 °C for 24 h in a vacuum drying oven. After being dried, the coal samples were stored in a desiccator for subsequent experiments.

The micropore structure parameters of coal samples were obtained from the method of CO_2 adsorption at 0 °C by the ASAP 2020 system (Micromeritics Instruments, USA). The micropore surface area and volume were estimated using a D–A model, as shown in Table 2. The pore size distribution (PSD) was calculated using a density functional theory (DFT) model. The PSDs were presented in Fig. 2. The three types of coal samples have similar micropore structure distributions. There are two peaks at 0.55 nm and 0.85 nm, which indicates that there are more micropores at these locations. Anthracite has a higher micropore content than gas coal and lignite.

Table 1 Equations, parameters and isosteric heat of the adsorption models

Models	Equations	Parameters	q_{st-cc2}
① Langmuir	$n_a = n_{\max}\frac{bf}{1+bf}$ $n_{\max} = n_{\max,0}\exp\left[\chi\left(1-\frac{T}{T_0}\right)\right]$ $b = b_\infty \exp\left(\frac{q}{RT}\right)$	$n_{\max,0}$ (mmol/g) b_∞ (MPa^{-1}) q (kJ/mol) χ (dimensionless)	$q + \frac{\chi RT^2(1+bf)}{T_0}$
② Langmuir–Freundlich	$n_a = n_{\max}\frac{(bf)^{1/t}}{1+(bf)^{1/t}}$ $b = b_\infty \exp\left(\frac{q}{RT}\right)$ $\frac{1}{t} = \frac{1}{t_0} + \alpha\left(1-\frac{T_0}{T}\right)$ $n_{\max} = n_{\max,0}\exp\left[\chi\left(1-\frac{T}{T_0}\right)\right]$	$n_{\max,0}$ (mmol/g^1) b_∞ (MPa) q (kJ/mol) χ (dimensionless) t_0 (dimensionless) α (dimensionless)	$q + \frac{t\chi RT^2}{T_0}\left[1+(bf)^{1/t}\right] - \alpha t R T_0 \ln(bf)$
③ Toth	$n_a = n_{\max}\frac{bf}{(1+(bf)^t)^{1/t}}$ $n_{\max} = n_{\max,0}\exp\left[\chi\left(1-\frac{T}{T_0}\right)\right]$ $b = b_\infty \exp\left(\frac{q}{RT}\right)$ $t = t_0 + \alpha\left(1-\frac{T_0}{T}\right)$	$n_{\max,0}$ (mmol/g) b_∞ (MPa^{-1}) q (kJ/mol) χ (dimensionless) t_0 (dimensionless) α (dimensionless)	$q + \frac{\chi RT^2}{T_0}\left(1+(bf)^t\right) + \frac{\alpha RT_0}{t}\left(\left(1+(bf)^t\right)\ln\left(\frac{bf}{(1+(bf)^t)^{1/t}}\right) - \ln(bf)\right)$
④ Unilan	$n_a = \frac{n_{\max}}{2s}\ln\left(\frac{1+be^sf}{1+be^{-s}f}\right)$ $b = b_\infty \exp\left(\frac{E_{\max}+E_{\min}}{2RT}\right)$ $n_{\max} = n_{\max,0}\exp\left[\chi\left(1-\frac{T}{T_0}\right)\right]$ $s = \frac{E_{\max}-E_{\min}}{2RT}$	$n_{\max,0}$ (mmol/g) b_∞ (MPa^{-1}) $E_{\max}$ (kJ/mol) $E_{\min}$ (kJ/mol) χ (dimensionless)	$\frac{E_{\max}+E_{\min}}{2} - \frac{(E_{\max}-E_{\min})(2+e^sbf+e^{-s}bf)}{2bf(e^s-e^{-s})} + \frac{(1-n_an_{\max}^{-1})(E_{\max}-E_{\min})(e^s+bf)(e^{-s}+bf)}{bf(e^s-e^{-s})} + \frac{2s\chi RT^2T_0^{-1}n_an_{\max}^{-1}(e^s+bf)(e^{-s}+bf)}{bf(e^s-e^{-s})}$
⑤ Dual-site Langmuir	$n_a = n_{\max}\left((1-\alpha)\frac{b_1f}{1+b_1f} + \alpha\frac{b_2f}{1+b_2f}\right)$ $b_1 = b_{\infty1}\exp\left(\frac{q_1}{RT}\right)$ $b_2 = b_{\infty2}\exp\left(\frac{q_2}{RT}\right)$	$n_{\max}$ (mmol/g) $b_{\infty1}$ (MPa^{-1}) $b_{\infty2}$ (MPa^{-1}) q_1 (kJ/mol) q_2 (kJ/mol) α (dimensionless)	$\frac{b_1q_1(1-\alpha)(1+b_2f)^2+b_2q_2\alpha(1+b_1f)^2}{b_1(1-\alpha)(1+b_2f)^2+b_2\alpha(1+b_1f)^2}$
⑥ Modified Dubinin–Astakhov	$n_a = n_{\max}\exp\left\{-\left[\frac{RT}{a+bT}\ln\left(\frac{f^{sat}}{f}\right)\right]^m\right\}$ $f^{sat} = p_c(T/T_c)^k$	$n_{\max}$ (mmol/g) a (kJ/mol) b (kJ/mol/K) m (dimensionless) k (dimensionless)	$RTk + a\left(\ln\frac{n_{\max}}{n_a}\right)^{1/m}$

Table 2 Properties of the coal samples

Coal number	Location	Coal type	$R_{o,max}$ (%)	Proximate (wt%)				Micropore parameters	
				M_{ad}	A_{ad}	V_{ad}	FC_{ad}	S (m^2/g)	V (cm^3/g)
#1	Chengzhuang Coal mine	Anthracite	2.37	0.72	13.88	7.54	77.86	236.40	0.094
#2	Beizu Coal mine	Gas coal	0.72	1.92	11.58	35.61	50.89	140.61	0.056
#3	Donghuai Coal mine	Lignite	0.58	3.17	42.02	27.96	26.85	101.00	0.041

$R_{o,max}$(%) mean maximum reflectance of vitrinite, *wt* weight percentage, M_{ad} moisture, air-drying base, A_{ad} ash yield, air-drying base, V_{ad} volatile matter, air-drying base, FC_{ad} fixed carbon content, air-drying base, S micropore specific surface area, V micropore volume

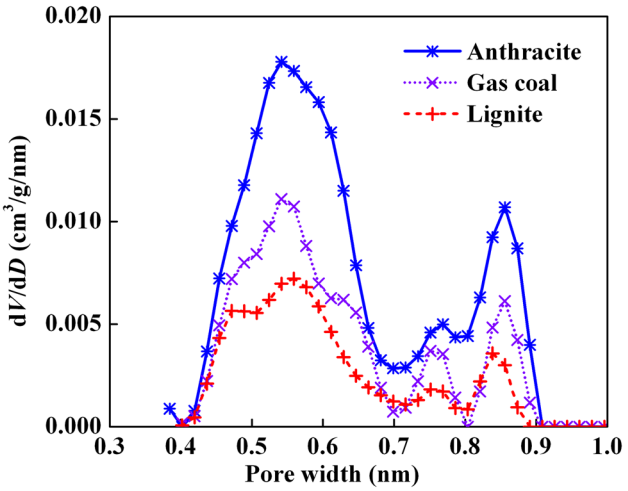

Fig. 2 Micropore size distribution profiles of the coal samples

3.2 Adsorption calorimetry experiments

The experimental device was designed to enable simultaneous measurements of the adsorption heat and isotherm, as shown in Fig. 3. A Tian Calvet Setaram C80 microcalorimeter was used to measure the adsorption heat. In the microcalorimeter, the adsorption cell and reference cell were connected and surrounded by hundreds of thermocouples in series to record the curves of the heat flux difference between adsorption and reference cells. Then, the heat difference Q_{exp} between the adsorption cell and the reference cell was calculated by integrating the curves of the heat flux difference. Due to the expansion of the gas from the dosing to the adsorption cell and the reference cell, the heat measured in the sample cell is subtracted from the one measured in the reference cell. The temperature accuracy of the microcalorimeter is 0.01 K, and the heat flux resolution is 0.10 μW. Before the experiment, the heat of fusion of standard reference indium (GBW(E) 130182) was measured for three times using a calorimeter to check the calorimeter precision. The measured average value is 28.574 J/g which agrees well with the standard value of 28.53 ± 0.30 J/g provided by Chinese National Standard Substances Center. In our experiment, the coal sample was put into the adsorption cell, whereas isometric steel balls were put into the reference cell. The heat measured directly in the experiment is the integral heat, and we have the following relations (Auroux 2013).

$$q_{st} = \frac{dQ_{\exp}}{dn} \tag{18}$$

where q_{st} is the isosteric heat, Q_{exp} is the integral heat, and n is the adsorption content.

Assuming that the isosteric heat varies linearly with the adsorption content between two adjacent gas injection steps, namely

$$q_{st} \approx q_{st,i} + \frac{(q_{st,i+1} - q_{st,i})}{(n_{i+1} - n_i)}(n - n_i)\ , n \in (n_i, n_{i+1}) \tag{19}$$

where $q_{st,i}$ is the isosteric heat at the equilibrium pressure p_i, n_i is the adsorption content at the equilibrium pressure p_i. The heat difference between two adjacent gas injection steps is as follows

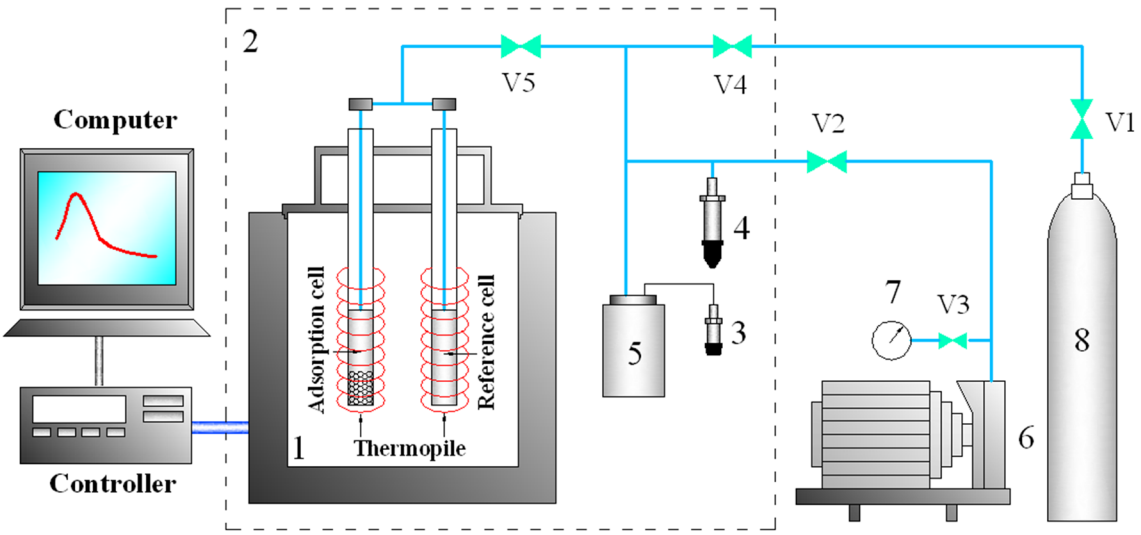

Fig. 3 Schematic diagram of the experimental apparatus: (1) C80 microcalorimeter; (2) thermostat; (3) temperature transmitter; (4) pressure transducer; (5) gas reservoir; (6) vacuum pump; (7) vacuum gauge; (8) gas cylinder; (V1–V5) valves

$$\begin{aligned}\Delta Q_{\exp} &= Q_{\exp,i+1} - Q_{\exp,i} \\ &= \int_{n_i}^{n_{i+1}} q_{st} dn \approx \frac{\left(q_{st,i} + q_{st,i+1}\right)}{2}\left(n_{i+1} - n_i\right) \\ &= \overline{q}_{st}\left(n_{i+1} - n_i\right)\end{aligned} \tag{20}$$

where $Q_{\exp,i}$ is the integral heat at the equilibrium pressure p_i, $\overline{q}_{st}$ is the isosteric heat when the adsorption content is equal to $(n_i + n_{i+1})/2$. So $\overline{q}_{st}$ can be calculated using the following equation:

$$\overline{q}_{st} = \frac{Q_{\exp,i+1} - Q_{\exp,i}}{n_{i+1} - n_i} = \frac{\Delta Q_{\exp,i}}{\Delta n_i} \tag{21}$$

The volumetric method was used to measure the adsorption isotherm. This device mainly consisted of a gas reservoir, a gas cylinder, a pressure transducer and a temperature sensor. The gas reservoir was connected to the microcalorimeter by 1/16 stainless-steel pipes and valves, and a thermostat was placed inside it. The pressure transducer with an accuracy of 0.01% of full scale in the range from vacuum to 10 MPa allows an accurate measurement of the gas phase pressure before and after adsorption. The temperature sensor is in the range from 243.14 to 423.15 K with an accuracy of 0.1 K. All experimental data were collected and logged into a computer.

The experimental procedure is described as follows:

(1) The air tightness of the entire system was checked. At the beginning of the experiment, 6 MPa He (99.9999% pure) was injected into the experimental device at room temperature, and the pressure was observed for 24 h to ensure good tightness.

(2) The void volume of the experimental device was measured. Volume calibration experiments were performed at testing temperatures through a detailed procedure, which was similar to the work of Ozdemir (2004). The void volumes of the entire device V_0 and gas reservoir V_g were determined by helium expansions from the gas reservoir to the adsorption cell and reference cell when the adsorption cell and reference cell were empty and the adsorption cell was filled with steel balls with a known reference volume, respectively. The procedure is as follows. Firstly, the helium gas at a pressure of p_0 was injected into the entire experimental device at room temperature. Then, valve 7 was closed and the gas reservoir was charged with fresh gas at pressure p_1. When valve 7 was open, a portion of the gas was transferred from the gas reservoir to the adsorption cell and reference cell until a new equilibrium pressure of p_2 was attained. At equilibrium, since there is no adsorption in empty cells and the total amount of gas was constant, we obtain

$$\frac{p_1 V_g}{z_{P_1} RT} - \frac{p_2 V_g}{z_{P_2} RT} = \frac{p_2(V_0 - V_g)}{z_{P_2} RT} - \frac{p_0(V_0 - V_g)}{z_{P_0} RT} \tag{22}$$

Therefore, the volume ratio of the entire device to the gas reservoir becomes

$$\frac{V_0}{V_g} = \frac{\frac{p_1}{z_{P_1}} - \frac{p_2}{z_{P_2}}}{\frac{p_2}{z_{P_2}} - \frac{p_0}{z_{P_0}}} + 1 = a \tag{23}$$

The gas expansion procedure was also repeated when the adsorption cell was filled with a known volume of steel balls. When the adsorption cell was loaded with steel balls, the volume ratio of the entire device to the gas reservoir is obtained from the mass balance as

$$\frac{V_0 - V_{sb}}{V_g} = \frac{\frac{p_1'}{z_{P_1'}} - \frac{p_2'}{z_{P_2'}}}{\frac{p_2'}{z_{P_2'}} - \frac{p_0'}{z_{P_0'}}} + 1 = b \tag{24}$$

Finally, the volumes of the gas reservoir and entire device were calculated using the following equation

$$V_g = \frac{V_{sb}}{a - b};\ V_0 = \frac{a}{a - b} V_{sb} \tag{25}$$

(3) The volume of the coal sample was measured. First, 5 g coal sample was put into the adsorption cell, and the experimental device was evacuated for 12 h. Then, step 2 was repeated, and the new void volume of the entire device V_1 was obtained. The volume of the coal sample V_c was calculated as $V_c = V_1 - V_0$. Then steel balls with the same volume were selected. The steel balls in the reference cell are all spherical with five different diameters, i.e. 1 mm, 2 mm, 3 mm, 4 mm and 5 mm. The volume of steel balls in the reference cell could be equal to the volume of the coal sample by adjusting the amount of steel balls with different diameters.

(4) Steel balls with volume V_c were put into the reference cell, and the experimental device was evacuated for 12 h. Then, the temperature of the microcalorimeter and thermostat was set to the desirable value of T. After the temperature change was below 0.1 K, the following procedure was employed for the estimation of the adsorption isotherms.

(5) The adsorption measurement began. Initially, the equilibrium pressure p_1 of the gas reservoir and the adsorption cell were recorded, and valve 5 between the gas reservoir and the microcalorimeter was closed. The gas

reservoir was charged with an appropriate content of methane and finally reached the equilibrium pressure p_2. Then, valve 5 between the gas reservoir and the microcalorimeter was opened, and the temperature, pressure and heat response data were recorded. When the pressure change was < 0.001 MPa and the heat flux was < 0.01 mW, equilibrium pressure p_3 of the gas reservoir and the adsorption cell was recorded. The excess adsorption content can be calculated from the mass balance as:

$$\Delta n_{ex} = \frac{p_1\left(V_1 - V_c - V_g\right)}{z_1 RT} + \frac{p_2 V_g}{z_2 RT} - \frac{p_3(V_1 - V_c)}{z_3 RT} \tag{26}$$

where p is the equilibrium pressure, T is the temperature, z is the compressibility factor (calculated by the NIST data base) and R is the gas constant. In particular, the measured adsorbed content at the end of the first step was determined from

$$\Delta n_{ex,1} = \frac{p_2 V_g}{z_2 RT} - \frac{p_3(V_1 - V_c)}{z_3 RT} \tag{27}$$

To get the isotherm, the above procedure was repeated for increasing injection pressure p_2 until all equilibrium pressure points were measured. Thus, the measured total adsorbed content at the end of the nth step is determined from

$$n_{ex} = \sum_{i=1}^{n} \Delta n_{ex,i} \tag{28}$$

and the measured total integral heat at the end of the nth step was determined from

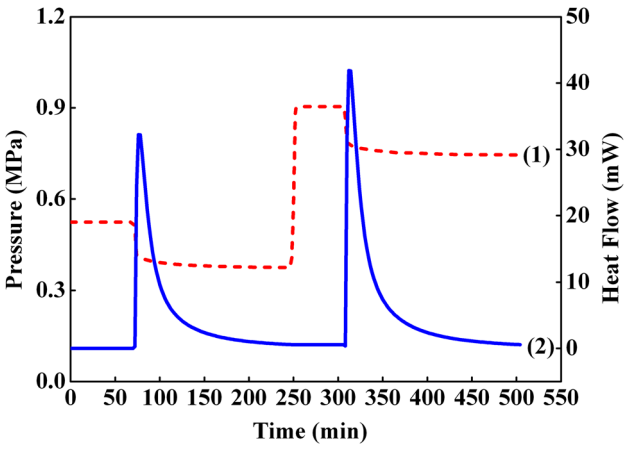

Fig. 4 Typical pressure (1) and heat response (2) changes after gas is dosed into the adsorption cell

$$Q_{ex} = \sum_{i=1}^{n} \Delta Q_{ex,i} \tag{29}$$

The typical curves of heat flux and pressure are shown in Fig. 4.

4 Results and discussion

4.1 Methane adsorption isotherms

The excess adsorption content n_{ex}, absolute adsorption content n_{a1} (specific volume of the adsorbed phase in Dubinin's method) and n_{a2} (specific volume of the adsorbed phase in Ozawa's method) are shown at three different temperatures in Fig. 5. The excess adsorption contents were almost equal to the absolute adsorption contents when the pressure was lower than 1 MPa. With the increase in pressure, the absolute adsorption content began to exceed the excess adsorption content. A larger specific volume of the adsorption phase indicates a larger absolute adsorption content. For the three coal samples, the adsorption content decreased with the increase in temperature from 303.15 to 323.15 K.

All absolute adsorption isotherms under different temperatures were simultaneously fitted by six types of adsorption models. The test data were processed using the Universal Global Optimization (UGO) method in 1stOpt 6.0 (7D-soft High Technology Inc., China). For the first four adsorption models, when the parameter $\chi = 0$, the fitting was performed first. In this paper, when $\chi = 0$, Langmuir model was denoted as the L-1 model (three fitted parameters). Similarly, Langmuir–Freundlich, Toth and Unilan models were denoted as the LF-1 model (five fitted parameters), T-1 model (five fitted parameters) and U-1 model (four fitted parameters), respectively. When parameter χ was also used as the fitting parameter, the fittings were reconducted. When $\chi \neq 0$, Langmuir, Langmuir–Freundlich, Toth and Unilan models were denoted as the L-2 model (four fitted parameters), LF-2 model (six fitted parameters), T-2 model (six fitted parameters) and U-2 model (five fitted parameters), respectively. Since the adsorption of CBM is supercritical and there is no saturated vapor pressure, the determination of the pseudo-saturation vapor pressure and k remains controversial for the modified D–A model (Srinivasan et al. 2011; Hao et al. 2014). In this paper, parameter k was first used as the fitting parameter; then, fittings were performed. The modified D–A model was denoted as the DA-1 model (five fitted parameters) in this paper. To avoid lose generality, the fittings were also performed when $k = 2$, 3, 4, 5, and 6. The corresponding modified D–A models were denoted as the DA-2, DA-3, DA-4, DA-5 and DA-6 models (four fitted parameters). In

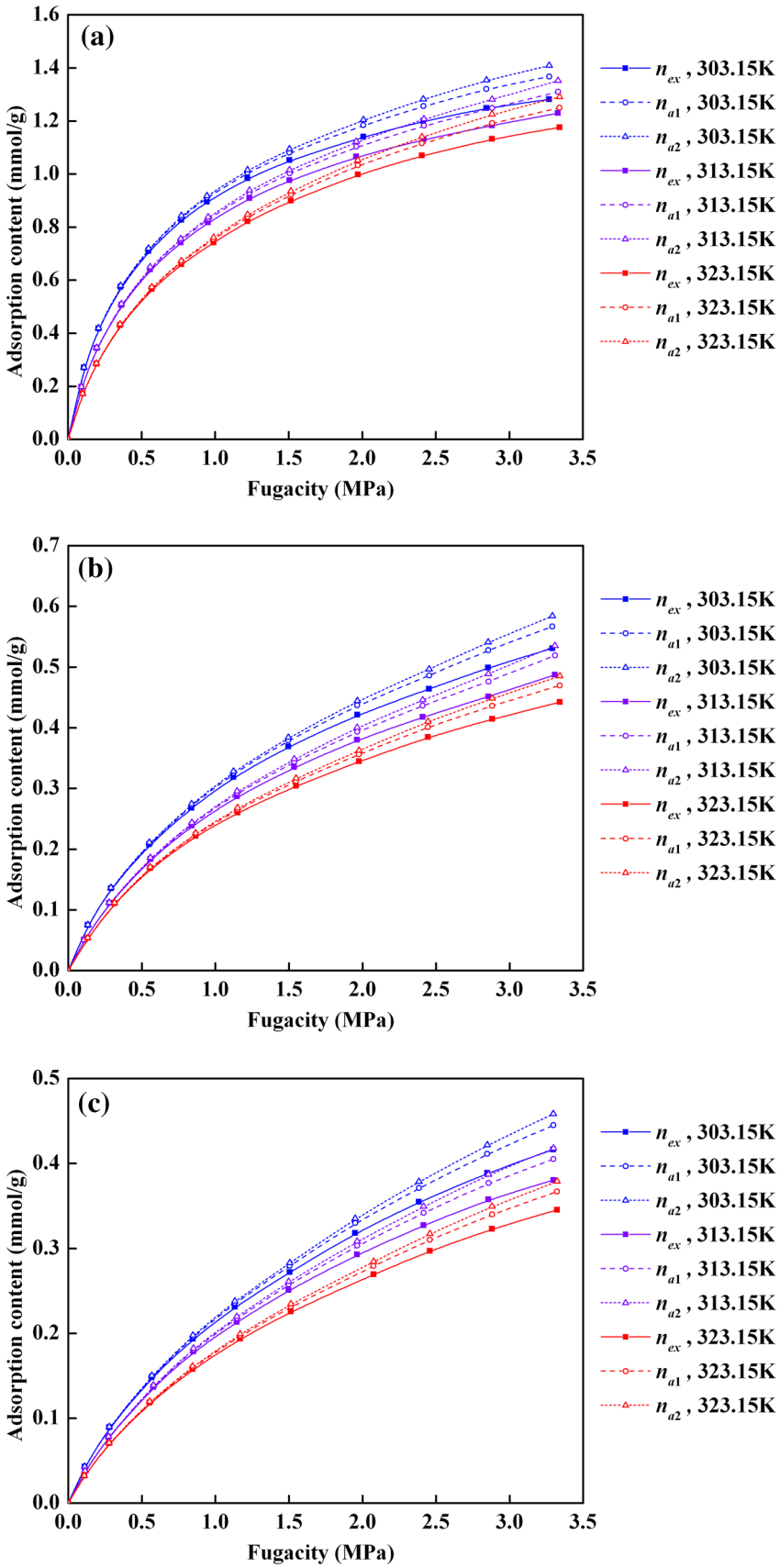

Fig. 5 Methane adsorption content in coal: **a** Anthracite, **b** Gas coal, **c** Lignite

addition, Dual-site Langmuir model in this paper is denoted as the DL model (six fitted parameters). The values of the fitted parameters and root mean square (RMS) are shown in Fig. S1 (see Supporting information). The RMS is defined as follows

$$\mathrm{RMS} = \left(\frac{\sum_{i=1}^{N} \left(n_i^{cal} - n_i^{\exp} \right)^2}{N} \right)^{0.5} \tag{30}$$

where N is the number of data points; n_i^{cal} and $n_i^{\exp}$ are the calculated and experimental adsorbed contents, respectively.

The fitted relative error is also used to evaluate the fitting goodness of the adsorption model between the predicted data and test data

$$\text{Relative error} = \frac{\left| n_{\text{fitted}} - n_{tested} \right|}{n_{\text{tested}}} \% \tag{31}$$

The comparison, log–log plot and relative error between fitting curve and test data for different adsorption models (specific volume of the adsorbed phase in Dubinin's method) are shown in Figs. S2–S4 (see Supporting information). Figure S2 shows that all six adsorption models can well fit the experimental data for the three coal samples. According to Fig. S4, most of the relative errors for the six adsorption models are within 5%, which also indicates that the experimental data were well fitted by these models. According to the RMS values in the Supporting information, a T-2 model with six fitted parameters obtained the best results for anthracite and lignite, and the DL model with six fitted parameters obtained the best results for gas coal. For the three coal samples, the worst fit result was the L-1 model with three fitted parameters. More fitted parameters in the model correspond to better the fitting results. Figure S3 shows that the fitting quality of models L-1 and L-2 is quite poor in the low-pressure section for the three coal samples. According to Fig. S4, models L-1 and L-2 for the three coal samples have large fitting error (above 15%) when the fugacity is < 0.5 MPa. Because models L-1 and L-2 have the simplest expresstions and the least numbers of the fitting parameters, the fitting quality is poorest for the three coal samples. Besides, Fig. S4 shows that the fitting errors of some low-pressure points of models LF-1, LF-2, U-1 and U-2 for gas coal and models U-1 and U-2 for lignite are greater than 10% when the fugacity is < 0.5 MPa. Due to the poor fitting in the low-pressure region, the adsorption heat values of these models may be inaccurate. In addition, Figs. S2–S4 show that the experimental isotherms of three coal samples can be well fitted by the modified D–A model for different k values. The above results can be also obtained for the specific volume of the adsorbed phase in Ozawa's method. The corresponding comparison, log–log plot and the relative error between fitting curve and test data are also shown in the Supporting information.

4.2 Isosteric heats of different adsorption models

The adsorption heat q_{st-c2} for different adsorption models and the calorimetric heat, which obtained from the absolute adsorption content n_{a1} are shown in Fig. 6. Firstly, Fig. 6 shows that models LF-1, LF-2, T-2, U-2 and DL for anthracite, models T-1, T-2 and DL for gas coal, and models LF-1 and DL for lignite have almost identical adsorption heat values, and these models all can well fit the experimental isotherms. The adsorption heat values of models L-1 and L-2 for anthracite are inconsistent with those of models LF-1, LF-2, T-2, U-2 and DL. Furthermore, the adsorption heat values of models L-1, L-2 and U-1 for gas coal are inconsistent with those of models T-1, T-2 and DL, and the adsorption heat values of models L-1, L-2, U-1 and U-2 for lignite are inconsistent with those of models LF-1 and DL. This inconsistency should be related to the poor fitting of models L-1 and L-2 for anthracite, models L-1, L-2 and U-1 for gas coal and models L-1, L-2, U-1 and U-2 for lignite when the fugacity is < 0.5 MPa. These results show that the fitting quality of the experimental isotherms affects the adsorption heat results of different models. Although the fitting errors of models LF-1, LF-2 and U-2 for gas coal are > 10% when the fugacity is < 0.5 MPa, the adsorption heat values of models LF-1, LF-2 and U-2 for gas coal are close to those of models T-1, T-2 and DL. This result also show that a too precise fitting may not be necessary for the calculation of the adsorption heat, because the experimental data may be affected by experimental errors. In addition, according to Figs. S2–S3 (see Supporting information), models T-1 and U-1 for anthracite and models LF-2, T-1 and T-2 for lignite can also well fit the experimental isotherms. However, Fig. 6 shows that the adsorption heat values of models T-1 and U-1 for anthracite are inconsistent with those of models LF-1, LF-2, T-2, U-2 and DL, and the adsorption heat values of models LF-2, T-1 and T-2 for lignite are inconsistent with those of models LF-1 and DL. These results show that even if some models well fit the isotherms data, different adsorption models may have inconsistent adsorption heat values. Finally, Fig. 6 shows that the adsorption heat results of the modified D–A model for different k values are inconsistent, although the experimental isotherms of three coal samples can be well fitted by the modified D–A model for different k values. With the increase in k, the heat at low coverage decreases, and the heat at high coverage increases for three coal samples. Overall, the theoretical adsorption heat based on various adsorption models may be uncertain, which may be related to the models or the quality of the data

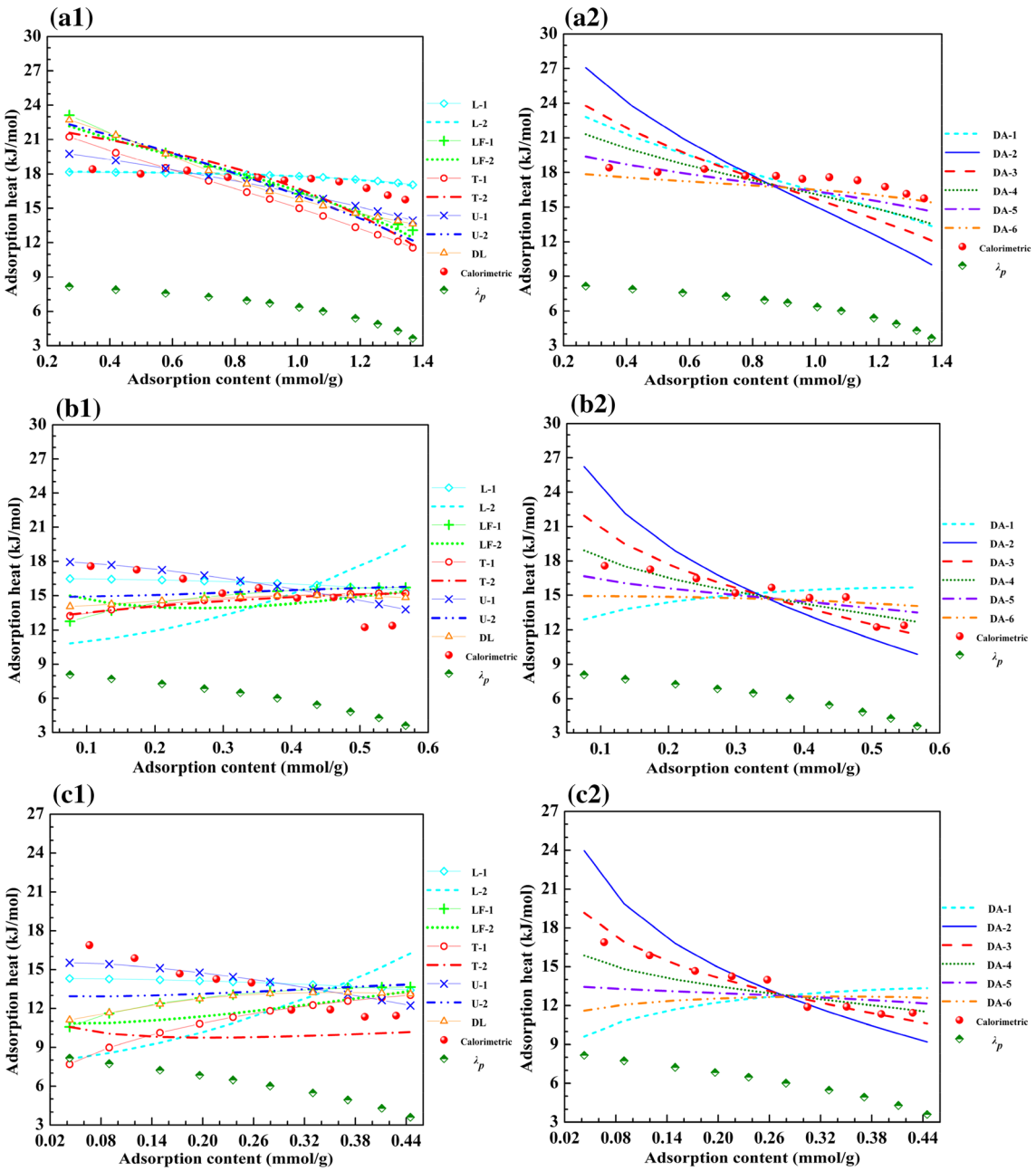

Fig. 6 Comparison between q_{st-c2} from the absolute adsorption data n_{a1} for different adsorption models and the calorimetric heat: **a1**–**a2** Anthracite, **b1**–**b2** Gas coal, **c1**–**c2** Lignite

and fitting. The above results can be also obtained for the specific volume of the adsorbed phase in Ozawa's method. The adsorption heat q_{st-c2} for different adsorption models and the calorimetric heat, which obtained from the absolute adsorption content n_{a2} are shown in Fig. S8 (see Supporting information).

Figure 6 shows all values of adsorption heat are 5–30 kJ/mol, so the methane adsorption obviously belongs to physical adsorption. According to Madani et al. (2015), the physical adsorption heat includes the condensation heat of adsorbed molecules q_{f-f} and the heat released by the interaction between the adsorbed molecules and the adsorbent molecules q_{f-s} .

$$q_{st} = q_{f-f} + q_{f-s} \tag{32}$$

Since methane is a nonpolar molecule, there is only a very weak dispersion force among the methane molecules. The coal molecules contain many polar and non-polar groups, so there is both dispersion and inductive forces between methane molecules and coal molecules. Since the experimental

temperature is above the supercritical temperature, there is no condensation heat. Therefore, the condensation heat of methane (λ_p is the absolute value of the condensation heat) under experimental pressure is calculated from the NIST REFPROP database, as shown in Fig. 6. The condensation heat of methane was shown to decrease with the increase in pressure and significantly lower than the adsorption heat. If the adsorbent is homogeneous, the heat released by the interaction between adsorbed molecules and adsorbent molecules should be approximately constant. However, if the adsorbent is heterogeneous, the heat released by the interaction between adsorbed molecules and adsorbent molecules should gradually reduce, and the molecule should be preferentially adsorbed at the position of higher adsorption energy with a smaller pore size (Madani et al. 2015). According to Fig. 2, coal has a heterogeneous pore structure, so the adsorption energy of the coal surface is nonuniform, and methane molecules should be preferentially adsorbed in places with smaller pores. Therefore, the heat released by interaction between methane and coal molecules should gradually decrease. Because the adsorbed molecules cannot fill the adsorption sites at the beginning of adsorption, the initial adsorption heat is the direct reaction of the interaction between adsorption molecules and the adsorbent surface (Madani et al. 2015). Because of the pore effect, the adsorbed molecules were first adsorbed in micropores, which are near the adsorbed molecules in terms of kinetic diameter. Because the adsorbed molecules contacted both sides of the pore wall, the isosteric heat was twice the isosteric heat of flat surface q. After the first class of pores was filled, adsorbed molecules were adsorbed in larger micropores, and since the adsorbed molecules completely interacted with one pore wall and partially with the other walls, the isosteric heat was $q - 2q$. After the second class of pores was filled, the adsorbed molecules were adsorbed in larger micropores. At this time, the methane molecules only interacted with one pore wall and the isosteric heat was equal to q. Since coal has a similar microcrystalline structure to graphite, the isosteric heat of methane on the surface of graphitized carbon black can be used to estimate the adsorption heat of methane in coal. The adsorption heat of methane on the carbon black surface was 12.23 kJ/mol and the dynamic diameter of molecular methane was 0.38 nm (Madani et al. 2016). Figure 2 shows that the coal samples contain more pores at 0.55 nm, so the initial adsorption heat should be 12.32–24.46 kJ/mol. In the early stage, the adsorption heat should decrease with the increase in adsorption content to almost 12.32 kJ/mol. Figure 6 shows that the calorimetric heats for the three coal samples are all within this range.

Because the calorimetric heat does not need to consider the different adsorption models, the calorimetric heats should be reasonably considered as the actural adsorption heat of the methane in coal. Although the theoretical adsorption heat may be related to the models, the actual adsorption heat of CBM in coal should be unique and independent of the adsorption models. Thus, a proposed adsorption model of CBM should well fit the experimental isotherms and extrapolate the observed heat. Figure 6 shows that the adsorption heat values of the modified D–A model can be close to that of the calorimetric heats for three coal samples when k is reasonably selected. Thus, the modified D–A model is selected as the best adsorption model of the methane in coal in this paper. By comparing the theoretical adsorption heat for different k values and the measured heat, the value of k and the pseudo-saturation vapor pressure can be determined to make the theoretical and measured adsorption heat consistent. Figure 6 shows that the best k values for anthracite, gas coal and lignite are 5, 4 and 3, respectively. The fitting parameters of the modified D–A model were shown in Table 3.

4.3 Effect of the adsorption isotherms on the isosteric heat

The modified D–A model (k is 5 for anthracite, 4 for gas coal and 3 for lignite) was used to fit the excess and absolute adsorption data, and the corresponding adsorption heats q_{st-cc1} are shown in Fig. 7. Figure 7 shows that the adsorption heat calculated by the excess adsorption data was higher than that calculated using the absolute adsorption data, and the difference increases at low pressure. A larger specific volume of the adsorption phase corresponds to a smaller adsorption heat. The calorimetric heat obtained from the excess adsorption data and absolute adsorption data is shown in Fig. 8. Figure 8 shows that the calorimetric heat obtained from the excess adsorption data is larger than that calculated using the absolute adsorption data, and the

Table 3 Summary of the fitting parameters of the modified D–A model

Models	Parameters	Anthracite	Gas coal	Lignite
Modified D–A (n_{a1})	n_{max} (mmol/g)	1.853310	1.076093	0.873619
	a (kJ/mol)	5.091227	4.679420	5.073225
	b (kJ/mol/K)	0.020935	0.008625	0.002345
	m (dimensionless)	2.252070	1.528587	1.326711
	k (dimensionless)	5	4	3
Modified D–A (n_{a2})	n_{max} (mmol/g)	1.985811	1.187705	0.960226
	a (kJ/mol)	4.187278	3.988743	4.445228
	b (kJ/mol/K)	0.022739	0.009612	0.003333
	m (dimensionless)	2.149721	1.462061	1.275349
	k (dimensionless)	5	4	3

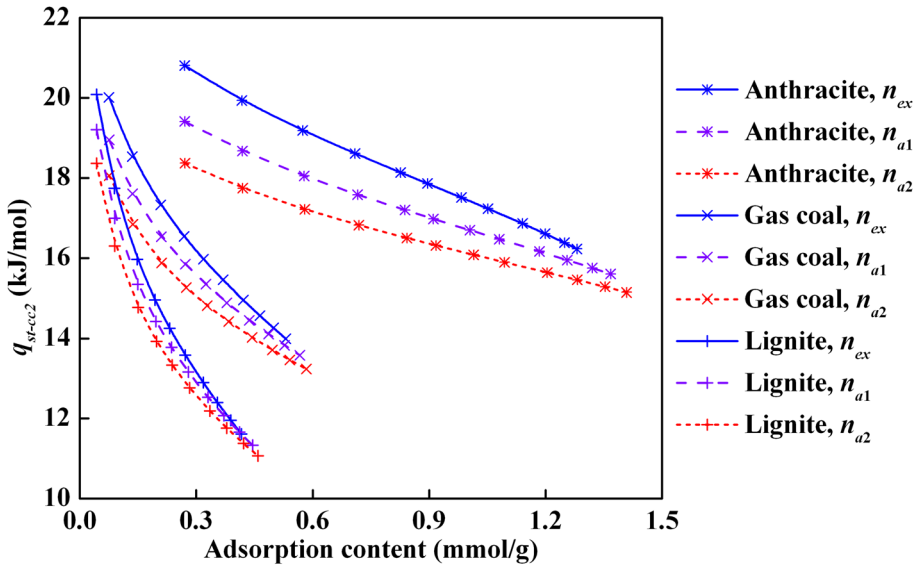

Fig. 7 Comparison between q_{st-cc2} from the excess adsorption data and q_{st-cc2} from the absolute adsorption data at 303.15 K

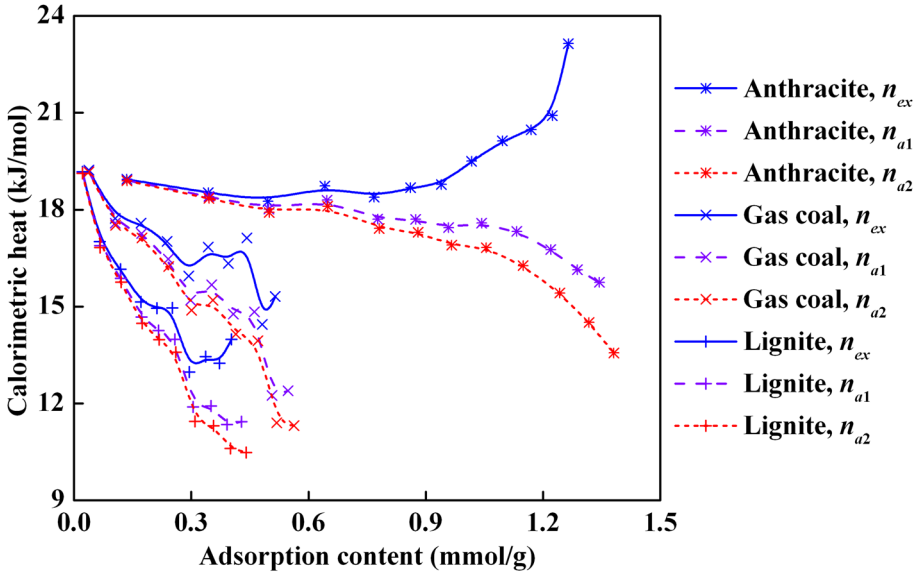

Fig. 8 Comparison between calorimetric heat obtained from the excess adsorption data and calorimetric heat obtained from the absolute adsorption data at 303.15 K

difference increases with the increase in pressure. A larger specific volume of the adsorption phase corresponds to a smaller calorimetric heat. Figure 8 shows that for anthracite, the calorimetric heats obtained using the excess adsorption data increases with the increase in adsorption content, and the adsorption heat calculated from the excess adsorption data was unreliable. So the absolute adsorption rather than excess adsorption should be used for the calculation of the adsorption heat.

4.4 Effect of temperature on the isosteric heat

The modified D–A model (k is five for anthracite, four for gas coal and three for lignite) was used to fit the absolute adsorption data (specific volume of the adsorbed phase in Ozawa's method) and adsorption heats q_{st-cc2} at three different temperatures, as shown in Fig. 9. Figure 9 shows the adsorption heat slightly increase with the increase in temperature. The difference in adsorption heat at adjacent temperature is small and can be considered invariant. The curves of the integral heats with the adsorption content measured by the microcalorimeter at different temperatures are shown in Fig. S9 (see Supporting information). The curves of the integral heat at different temperatures were almost coincident, so there was little change in the adsorption heat at the experimental temperature. This result reasonably occurred because the interaction between methane molecules and the coal surface is mainly caused by the inductive force and dispersion force, and the induced force and dispersion force are independent of temperature. When the range of temperature

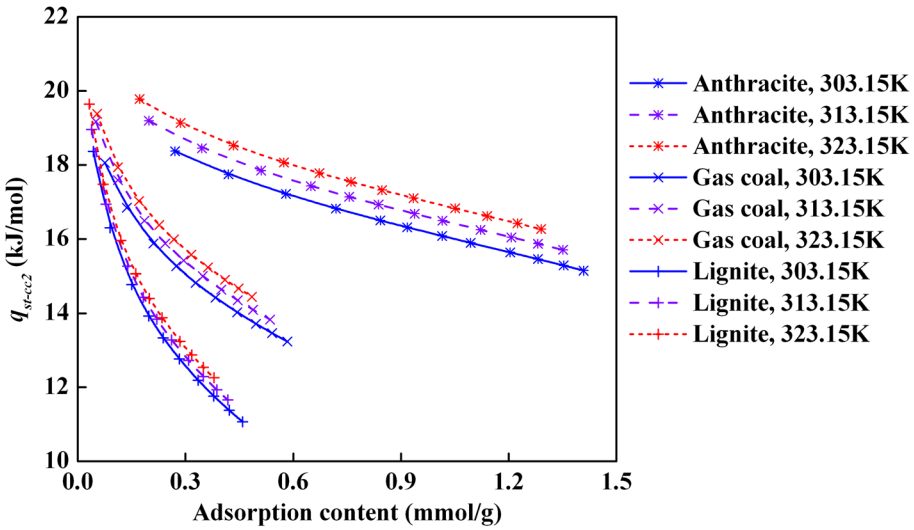

Fig. 9 q_{st-cc2} obtained from the absolute adsorption data (adsorption phase volume from Formula [17]) for the modified D–A model at different temperatures

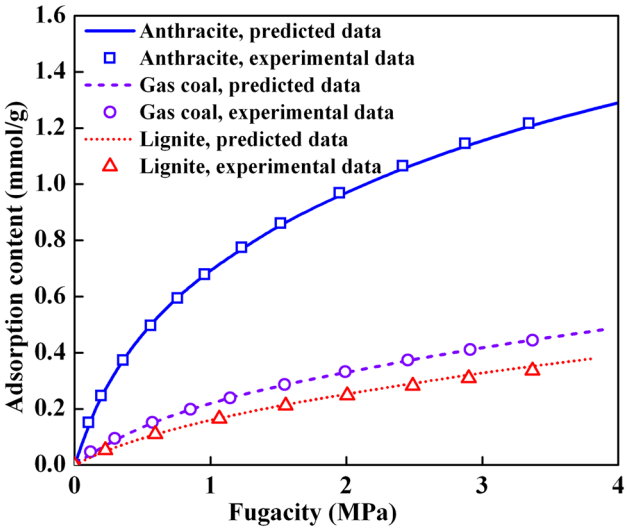

Fig. 10 Predicted adsorption isotherms at 333.15 K using the adsorption thermodynamic method

changes is small, the adsorption heat can be considered constant with temperature. For adjacent temperatures T_1 and T_2, according to Eq. (7) for a certain adsorption content n_a,

$$q_{st-cc2} = -R\frac{\ln f_2 - \ln f_1}{1/T_2 - 1/T_1} \tag{33}$$

When we know the adsorption heat and isotherm at T_1, we can calculate f_2 at T_2 for a certain adsorption content n_a as follows

$$f_2 = f_1 \exp\left(\frac{q_{st-cc2}}{R}\left(1/T_1 - 1/T_2\right)\right) \tag{34}$$

The adsorption content at other temperatures can be extrapolated according to one temperature isotherm. The adsorption content at 333.15 K is calculated according to the adsorption heat data and adsorption isotherm at 323.15 K, as shown in Fig. 10. The adsorption content is consistent with the experimental data. This method is simple, effective, and can satisfy engineering applications.

5 Conclusions

In this work, four types of adsorption heat were compared, and the effect of the volume of the adsorbed phase on the adsorption heat was analyzed. Then, the analytical expressions of the isosteric heat for six adsorption isotherm models were derived. The volumetric method of adsorption was combined with the microcalorimetry system to measure the adsorption content and adsorption heat at different temperatures. Then, the theoretical adsorption heats calculated from different adsorption models and calorimetric heats were compared. Combined with the pore size analysis of coal samples, we have found that the adsorption heat of coal samples decreases with the increase in adsorption content, and the calorimetric heat results for all coal samples are consistent with this rule. However, the theoretical adsorption heat obtained by different adsorption models exhibits different trends. In some cases, even if the models well fit the experimental isotherms, the adsorption heat values may be inconsistent. For all coal samples, the modified D–A model can well fit the experimental isotherms and obtain similar results of calorimetric heat. By comparing the theoretical adsorption heat for different k values and the measured heat, the value of k and the pseudo-saturation vapor pressure can be determined to make the theoretical and measured adsorption heat consistent. The calculated adsorption heats and calorimetric heats obtained from the excess adsorption content are higher than those obtained from absolute

adsorption content, and a larger specific volume of the adsorption phase corresponds to a smaller adsorption heat. In addition, the adsorption heat hardly changes over a small temperature range. In engineering practice, the adsorption isotherms at adjacent temperatures can be predicted according to the isosteric heat of adsorption.

Acknowledgements This work was supported by the National Key Research and Development Program of China (2018YFC0808100), the Fundamental Research Funds for the Central Universities (Grant No. 2015XKZD03), the Program for Changjiang Scholars and Innovative Research Team in University (Grant No. IRT_17R103).

References

Askalany, A.A., Saha, B.B.: Towards an accurate estimation of the isosteric heat of adsorption—a correlation with the potential theory. J. Colloid Interface Sci. **490**, 59–63 (2017)

Auroux, A.: Calorimetry and Thermal Methods in Catalysis. Springer Series in Materials Science, pp. 30–32. Springer, Berlin, (2013)

Baran, P., Zarębska, K., Nodzeński, A.: Energy aspects of CO_2 sorption in the context of sequestration in coal deposits. J. Earth Sci. **25**(4), 719–726 (2014)

Bhadra, S.J., Ebner, A.D., Ritter, J.A.: On the use of the dual process Langmuir model for predicting unary and binary isosteric heats of adsorption. Langmuir **28**, 6935–6941 (2012)

Bimbo, N., Sharpe, J.E., Ting, V.P., et al.: Isosteric enthalpies for hydrogen adsorbed on nanoporous materials at high pressures. Adsorption **20**, 373–384 (2014)

Brandani, S., Mangano, E., Luberti, M.: Net, excess and absolute adsorption in mixed gas adsorption. Adsorption **23**, 569–576 (2017)

Bülow, M., Shen, D., Jale, S.: Measurement of sorption equilibria under isosteric conditions: the principles, advantages and limitations. Appl. Surf. Sci. **196**, 157–172 (2002)

Busch, A., Gensterblum, Y.: CBM and CO_2-ECBM related sorption processes in coal: a review. Int. J. Coal Geol. **87**(2), 49–71 (2011)

Bustin, R.M., Clarkson, C.R.: Geological controls on coalbed methane reservoir capacity and gas content. Int. J. Coal Geol. **38**(1–2), 3–26 (1998)

Chakraborty, A., Saha, B.B., Koyama, S.: On the thermodynamic modeling of the isosteric heat of adsorption and comparison with experiments. Appl. Phys. Lett. **89**, 171901 (2006)

Chattaraj, S., Mohanty, D., Kumar, T., Halder, G.: Thermodynamics, kinetics and modeling of sorption behaviour of coalbed methane: a review. J. Unconv. Oil Gas Resour. **16**, 14–33 (2016)

Chikatamarla, L., Crosdale, P.J.: Heat of methane adsorption of coal: implications for pore structure development. In Proceedings of the International Coalbed Methane Symposium, University of Alabama, Tuscaloosa, AL, May 14–18, pp. 151–162: (2001)

Do, D.D.: Adsorption Analysis: Equilibria and Kinetics. Imperial College Press, London (1998)

Do, D.D., Nicholson, D., Do, H.D.: On the Henry constant and isosteric heat at zero loading in gas phase adsorption. J. Colloid Interface Sci. **324**, 15–16 (2008)

Duan, S., Gu, M., Du, X., Xian, X.: Adsorption equilibrium of CO_2 and CH_4 and their mixture on Sichuan Basin shale. Energy Fuels **30**, 2248–2256 (2016)

Dubinin, M.M.: The potential theory of adsorption of gases and vapors for adsorbents with energetically nonuniform surfaces. Chem. Rev. **60**(2), 235–241 (1960)

Dutka, B., Kudasik, M., Pokryszka, Z., Skoczylas, N., Topolnicki, J., Wierzbicki, M.: Balance of CO_2/CH_4 exchange sorption in a coal briquette. Fuel Process. Technol. **106**(0), 95–101 (2013)

Hao, S., Chu, W., Jiang, Q., Yu, X.: Methane adsorption characteristics on coal surface above critical temperature through Dubinin–Astakhov model and Langmuir model. Colloids Surf. A **444**, 104–113 (2014)

Horikawa, T., Zeng, Y., Do, D.D., Sotowa, K., Avila, J.R.A.: On the isosteric heat of adsorption of non-polar and polar fluids on highly graphitized carbon black. J. Colloid Interface Sci. **439**, 1–6 (2015)

Kim, H.J., Shi, Y., He, J., Lee, H.-H., Lee, C.-H.: Adsorption characteristics of CO_2 and CH_4 on dry and wet coal from subcritical to supercritical conditions. Chem. Eng.J. **171**, 45–53 (2011)

Kloutse, A.F., Zacharia, R., Cossement, D., et al.: Isosteric heat of hydrogen adsorption on MOFs: comparison between adsorption calorimetry, sorption isosteric method, and analytical models. Appl. Phys. A **121**, 1417–1424 (2015)

Liang, L., Xiong, J., Liu, X., Luo, D.: An investigation into the thermodynamic characteristics of methane adsorption on different clay minerals. J. Nat. Gas Sci. Eng. **33**, 1046–1055 (2016)

Liu, J., Wang, C., He, X., Li, S.: Infrared measurement of temperature field in coal gas desorption. Int. J. Min. Sci. Technol. **24**, 57–61 (2014)

Madani, S.H., Sedghi, S., Biggs, M.J., Pendleton, P.: Analysis of adsorbate–adsorbate and adsorbate–adsorbent interactions to decode isosteric heats of gas adsorption. ChemPhysChem **16**, 3797–3805 (2015)

Madani, S.H., Hu, C., Silvestre-Albero, A., et al.: Pore size distributions derived from adsorption isotherms, immersion calorimetry, and isosteric heats: a comparative study. Carbon **96**, 1106–1113 (2016)

Moore, T.A.: Coalbed methane: a review. Int. J. Coal Geol. **101**(0), 36–81 (2012)

Myers, A.L., Monson, P.A.: Physical adsorption of gases: the case for absolute adsorption as the basis for thermodynamic analysis. Adsorption **20**, 591–622 (2014)

Nieszporek, K.: Theoretical description of the calorimetric effects accompanying the mixed-gas adsorption equilibria by using the ideal adsorbed solution theory. Langmuir **18**(18), 9334–9341 (2002)

Ning, P., Li, F., Yi, H., et al.: Adsorption equilibrium of methane and carbon dioxide on microwave-activated carbon. Sep. Purif. Technol. **98**(39), 321–326 (2012)

Ozawa, S., Kusumi, S., Ogino, Y.: Physical adsorption of gases at high pressures(IV): an improvement of the Dubinin-Astakhov adsorption equation. J. Colloid Interface Sci. **56**(1), 83–91 (1976)

Ozdemir, E.: Chemistry of the adsorption of carbon dioxide by Argonne Premium coals and a model to simulate CO_2 sequestration in coal seams. Ph. D. dissertation. School of Engineering, University of Pittsburgh, Pittsburgh, PA: (2004)

Pan, H., Ritter, J.A., Balbuena, P.B.: Examination of the approximations used in determining the isosteric heat of adsorption from the Clausius-Clapeyron equation. Langmuir **14**, 6323–6327 (1998)

Richard, M.A., Bénard, P., Chahine, R.: Gas adsorption process in activated carbon over a wide temperature range above the critical point. Part 1: modified Dubinin-Astakhov model. Adsorption **15**, 43–51 (2009)

Siperstein, F., Gorte, R.J., Myers, A.L.: A new calorimeter for simultaneous measurements of loading and heats of adsorption from gaseous mixtures. Langmuir **15**, 1570–1576 (1999)

Srinivasan, K., Saha, B.B., Ng, K.K., et al.: A method for the calculation of the adsorbed phase volume and pseudo-saturation pressure from adsorption isotherm data on activated carbon. Phys. Chem. Chem. Phys. **13**, 12559–12570 (2011)

Stadie, N.P., Murialdo, M., Ahn, C.C., Fultz, B.: Anomalous isosteric enthalpy of adsorption of methane on zeolite-templated carbon. J. Am. Chem. Soc. **135**(3), 990–993 (2013)

Tang, X., Ripepi, N.: High pressure supercritical carbon dioxide adsorption in coal: adsorption model and thermodynamic characteristics. J. CO2 Util. **18**(18), 189–197 (2017)

Tang, X., Wang, Z., Ripepi, N., Kang, B., Yue, G.: Adsorption affinity of different types of coal: mean isosteric heat of adsorption. Energy Fuels **29**, 3609–3615 (2015)

Tang, X., Ripepi, N., Stadie, N.P., et al.: Thermodynamic analysis of high pressure methane adsorption in Longmaxi shale. Fuel **193**, 411–418 (2017)

White, C.M., Smith, D.H., Jones, K.L., et al.: Sequestration of carbon dioxide in coal with enhanced coalbed methane recovery-a review. Energy Fuels **19**, 659–724 (2005)

Wu, S., Tang, D., Li, S., Chen, H., Wu, H.: Coalbed methane adsorption behavior and its energy variation features under supercritical pressure and temperature conditions. J. Pet. Sci. Eng. **146**, 726–734 (2016)

Yue, G., Wang, Z., Tang, X., Li, H., Xie, C.: Physical simulation of temperature influence on methane sorption and kinetics in coal (II): Temperature evolvement during methane adsorption in coal measurement and modeling. Energy Fuels **29**, 6355–6362 (2015)

Zimmermann, W., Keller, J.U.: A new calorimeter for simultaneous measurement of isotherms and heats of adsorption. Thermochim. Acta **405**, 31–41 (2003)